Cationic Porphyrins Promote the Formation of i-Motif DNA and Bind Peripherally by a Nonintercalative Mechanism†

Oleg Yu. Fedoroff,‡ Anupama Rangan,§ Violetta V. Chemeris,‡ and Laurence H. Hurley*,‖

Drug Dynamics Institute and Division of Medicinal Chemistry, College of Pharmacy, The University of Texas at Austin, Austin, Texas 78712, Arizona Cancer Center, The University of Arizona, Tucson, Arizona 85724, and College of Pharmacy, The University of Arizona, Tucson, Arizona 85721

Received July 5, 2000; Revised Manuscript Received September 28, 2000

ABSTRACT: Telomeric C-rich strands can form a noncanonical intercalated DNA structure known as an i-motif. We have studied the interactions of the cationic porphyrin 5,10,15,20-tetra-(*N*-methyl-4-pyridyl)-porphine (TMPyP4) with the i-motif forms of several oligonucleotides containing telomeric sequences. TMPyP4 was found to promote the formation of the i-motif DNA structure. On the basis of ^{1}H NMR studies, we have created a model of the i-motif−TMPyP4 complex that is consistent with all the available experimental data. Two-dimensional NOESY data prompted us to conclude that TMPyP4 binds specifically to the edge of the intercalated DNA core by a nonintercalative mechanism. Since we have shown that TMPyP4 binds to and stabilizes the G-quadruplex form of the complementary G-rich telomeric strand, this study raises the intriguing possibility that TMPyP4 can trigger the formation of unusual DNA structures in both strands of the telomeres, which may in turn explain the recently documented biological effects of TMPyP4 in cancer cells.

Simple repetitive DNA sequences are abundant in eukaryotic genomes. Some of these sequences, for example, telomeric repeats, have important biological functions (*1*). Human telomeric DNA is composed of multiple repeats of TTAGGG on one strand and CCCTAA on the other. The G-rich strand is longer and has a single-strand overhang of approximately 100−150 base pairs (*2*, *3*). The single-stranded nature and G-rich composition of this overhang allow formation of a G-quadruplex secondary structure (*4*), although these structures so far have not been identified in vivo. G-Quadruplex DNA formed by telomeric or other genomic DNA sequences has attracted numerous investigations (reviewed in refs *4* and *5*). Telomeric G-quadruplex has been shown to interfere with telomerase activity and was therefore proposed as a target for anticancer drug design (*6*−*8*). In addition, several proteins have been identified that bind specifically to G-quadruplexes or perform selective enzymatic activity on G-quadruplex substrates (*9*−*16*). However, except for the short 3′-end G-rich overhang, all chromosomal DNAs potentially capable of forming G-quadruplexes are masked by their Watson−Crick complementary C-rich strand DNA. Formation of a G-quadruplex structure within genomic DNA should therefore be coupled with the self-organization of the complementary C-rich strand (*17*, *18*).

Several C-rich oligomers have been shown to form a C·C+ tetraplex, termed an i-motif, at low or even neutral pH (*19*−*24*). These structures consist of four DNA strands arranged in two parallel duplexes "zipped" together in an antiparallel orientation (Figure 1A). High-resolution NMR and crystallographic studies have identified the structural details of i-motif DNA and provided insights into factors governing its stability (*24*−*31*). The i-motif has a much shorter history compared to other noncanonical DNA structures such as DNA triplexes or G-quadruplexes. Not surprisingly, reports of i-motif interactions with either proteins or low-molecular weight ligands have not yet appeared, and to our knowledge, we present here the first such study. We chose the cationic porphyrin 5,10,15,20-tetra-(*N*-methyl-4-pyridyl)porphine (TMPyP4)[1] (Figure 1B) as the lead candidate. The rationale for this is the recent finding of chromosomal destabilization caused by TMPyP4, which we suspect may be mediated through the formation of noncanonical DNA structures (*32*).

MATERIALS AND METHODS

Oligomer Synthesis for PAGE Studies and TMPyP4 Preparation. 5′-AACCCC-3′ was synthesized on a DNA synthesizer (PerSeptive Biosystems Expedite 8909). The oligomer was purified by 20% denaturing polyacrylamide gel electrophoresis (PAGE), diluted to 100 nM, and dispensed into small aliquots. Approximately 200 ng was 5′-end-labeled with ^{32}P using T4 polynucleotide kinase (New England Labs) and subsequently purified by 20% denaturing PAGE. The chloride salt of TMPyP4 was purchased from Aldrich and used without further purification. A 10 mM stock solution of TMPyP4 prepared in distilled water was stored

† This work was supported by a grant from the National Institutes of Health (CA-49751) and a National Cooperative Drug Discovery Group grant (CA-67760).

* To whom correspondence should be addressed. Telephone: (520) 626-5622. Fax: (520) 626-5623. E-mail: hurley@pharmacy.arizona.edu.

‡ Drug Dynamics Institute, The University of Texas at Austin.

§ Division of Medicinal Chemistry, College of Pharmacy, The University of Texas at Austin.

‖ The University of Arizona.

[1] Abbreviation: TMPyP4, 5,10,15,20-tetra-(*N*-methyl-4-pyridyl)-porphine.

10.1021/bi001528j CCC: $19.00
Published on Web 11/10/2000

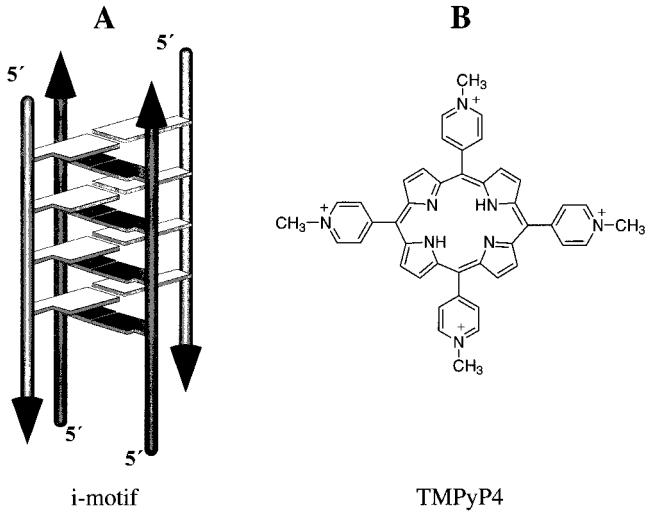

FIGURE 1: (A) Schematic representation of the i-motif structure (based on Figure 1 in ref *53*). (B) Chemical structure of TMPyP4.

at −20 °C and diluted to working concentrations immediately before use.

Assay of DNA Secondary Structure by Native Gel Shift PAGE. ^{32}P-end-labeled oligomer at a concentration of 100 nM was heated to 95 °C for 5 min in 1 μM buffer [10 mM Tris·acetate and 1 mM EDTA (pH 4.5)]. After the DNA was cooled to room temperature, 2 μL of stock TMPyP4 was dispensed to each sample to produce specified concentrations in a total volume of 20 μL. Reaction mixtures were incubated at room temperature for 1 h. After incubation, 2 μL of gel loading solution (50% glycerol, 0.25% bromophenol blue, and 0.25% xylene cyanol) was added to each mixture. Aliquots (8 μL) of each sample were analyzed by native 16% PAGE at pH 4.5 (the gel was prerun for 30 min). Electrophoresis proceeded for 22 h at 4 °C. Gels were dried and then visualized and quantified on a PhosphorImager (Molecular Dynamics model 445 SI).

NMR Sample Preparations. DNA oligonucleotides were synthesized on a 15 μM scale on a PerSeptive Biosystems Expedite 8909 automatic DNA synthesizer, purified by reverse phase HPLC on a C18 column (Dynamax-300A), and dialyzed extensively, first against a 10 mM KCl solution and then against deionized water. Solid supports and phosphoramidites were purchased from Glen Research and PerSeptive Biosystems, respectively.

NMR Spectroscopy. NMR experiments were performed on a Varian UNITY plus 500 MHz spectrometer. All titration experiments were carried out at 15 °C in a 90% H_2O/10% D_2O solution containing 150 mM KCl, 25 mM KH_2PO_4, and 1 mM EDTA. The pH values of all samples were in the range of 5.8−6.0. The optimal experimental conditions for i-motif formation require acidic pH, preferably <5.0 (*20*, *21*). We chose the higher-pH range to keep the experimental conditions as close to physiological ones as possible without greatly compromising the i-motif stability.

A standard 1-1 echo pulse sequence with a maximum excitation centered at 12.0 ppm was used for water suppression. Thirty-two scans were acquired for each spectrum with a relaxation delay of 2 s. Two-dimensional NOESY spectra of exchangeable protons were collected at 15 °C in the TPPI mode with a mixing time of 200 ms using 2048 complex points in t_2 and 1024 t_1 experiments. NOESY and DQF-COSY spectra of nonexchangeable protons were collected at 15 °C in a phase-sensitive mode using 2048 complex points in t_2 and 512 pairs of real and imaginary t_1 experiments. Two mixing times of 150 and 200 ms were used in the NOESY experiments. NMR data were processed and analyzed using the FELIX program (Molecular Simulations, Inc.).

Model Building and Molecular Dynamics Refinement. The starting structure for molecular modeling of $(dAACCCC)_4$ and its complex with porphyrin was the published crystal structure with a 5′-end outermost C·C+ base pair (*30*). The only adjustment to the starting structure was the setting of the torsional angles on the A2-C3 steps to values typical for B-form DNA. The rationale for this was the observed base stacking between A2 and C3 residues. Several sequential NOEs have been detected and assigned for the A2-C3 step, namely, C3H6−A2H1′, C3H6−A2H2″, C3H6−A2H2′, C3H6−A2H3′, and C3H5′/H5″−A2H1′. For all of them, the intensities were very close to the respective NOE observed previously in studies of standard B-form DNA duplexes. Restrained molecular dynamics (10 ps at 200 K) and mechanics (2000 cycles of conjugated gradient minimization) were subsequently used for energy refinement of the models (DISCOVER program with the AMBER force field, Molecular Simulations, Inc.). After the initial refinement of the free DNA structure, the porphyrin molecule was manually placed in the proposed binding site. The model was subjected to a combination of restrained molecular dynamics (20 ps at 250 K) and conjugate gradient refinement. Five independent runs were performed for better sampling of conformational space. The distance restraints were taken from NOESY cross-peaks and assigned as either strong (2.0−2.8 Å), medium (2.5−4.0 Å), or weak (3.5−5.5 Å). The cytosine H5−H6 cross-peaks were used as a reference. The isolated spin approximation was used to estimate distances. No attempts were made to employ the relaxation matrix refinement since NMR data indicate that the dynamical equilibrium between two binding sites and an accurate estimation of the correlation time for intermolecular cross relaxations were not possible. Any attempts to derive distance restraints more accurately could produce misleading and potentially biased results due to the highly dynamic nature of the complex.

UV Spectrometry. Absorbance spectra were measured on a Varian Cary 3E UV−visible spectrophotometer in 1 cm cells. For binding experiments, the free porphyrin solution (1.5−2.5 μM) was titrated with the solution containing a mixture of DNA ([DNA] = 200−400 μM in the tetraplex) and porphyrin. The porphyrin concentration in the mixture was exactly the same as in the free porphyrin solution so that the constant porphyrin concentration could be maintained during the course of the titration. Spectra were recorded after incubation for 5 min. To decrease the level of porphyrin association on a glass surface, we used the lowest possible concentrations. Experiments have been repeated with different porphyrin concentrations to ensure that this problem does not affect the reliability of the binding data.

RESULTS

There have been a number of reports of i-motif formation by different oligonucleotides containing stretches of three or more cytosines (*20*−*31*). We focused our studies on the

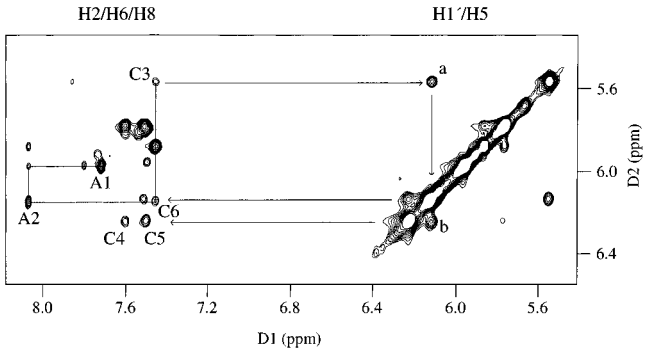

FIGURE 2: Assignments of H2/H6/H8−H1′/H5 protons of $(dAACCCC)_4$. Intraresidue H6/H8 cross-peaks are labeled with residue numbers and connected by arrows with pseudosequential intermolecular H1′−H1′ cross-peaks. The sequential connectivity in the A1-A2-C3 fragment is shown with solid lines.

human telomeric C-strand repeats dCCCAAT and dAATCCC and the *Tetrahymena* telomeric repeat dAACCCC. The latter has been included because of its greater stability and more unusual crystallographic structure (*30*).

NMR Assignments and Solution Structure of $(dAACCCC)_4$. The starting point for any NMR spectroscopy study of drug−DNA interactions is the spectral assignment of unbound DNA. The i-motif form of the dAACCCC oligonucleotide has not been studied previously by NMR. Figure 2 shows the H2/H6/H8−H1′/H5 expansion of the two-dimensional NOESY spectra. We have been able to make a complete proton assignment using the procedure of Gueron and coworkers (*19*−*21*, *24*). An important spectral feature of $(dAACCCC)_4$ is the strong interresidue H1′−H1′ cross-peaks, which are regarded as a signature of the i-motif structure (*19*, *24*). Spectral dispersion of H1′ protons allows us to identify two out of three possible H1′−H1′ cross-peaks: the C3H1′−C6H1′ and C6H1′−C4H1′ cross-peaks shown in Figure 2 (labeled a and b, respectively) and connected by arrows with the corresponding H6−H1′ intranucleotide cross-peaks, labeled C3 and C6, respectively. The chemical shift overlap between C4H1′ and C5H1′ places the C4H1′−C5H1′ cross-peak on the diagonal.

The $(dAACCCC)_4$ has been shown to be in two different forms in the crystal (*30*). In one form, the outermost C·C+ pairs are from the 5′-end of each strand, and in the other form, the outermost C·C+ pairs are from the 3′-ends. According to previous studies, these different intercalation topologies should have quite different NMR proton resonance frequencies (*33*); however, only one set of NMR signals for the i-motif form of $(dAACCCC)_4$ has been detected, which indicates the presence of a single i-motif topology in solution. According to our assignment, the solution form of $(dAACCCC)_4$ is the one with 5′-end outermost C·C+ pairs.

There is a clear sequential connectivity between the A1, A2, and C3 protons. This connectivity can also be traced in the H6/H8−H3′ and H6′/H8−H2′/H2″ regions (spectra not shown). Molecular modeling of the $(dAACCCC)_4$ structure using NOE-derived distance restraints argues for strong stacking interactions between A2 and C3. This is in contrast to the crystal structure of $(dAACCCC)_4$, where peculiar crystal packing places adenines in a specific intermolecular cluster in an orthogonal direction to the cytosines of the i-motif core (*30*). Except for adenine stacking, the solution structure of $(dAACCCC)_4$ was found to be very close to the crystal structure, and we decided not to discuss it in detail in this paper.

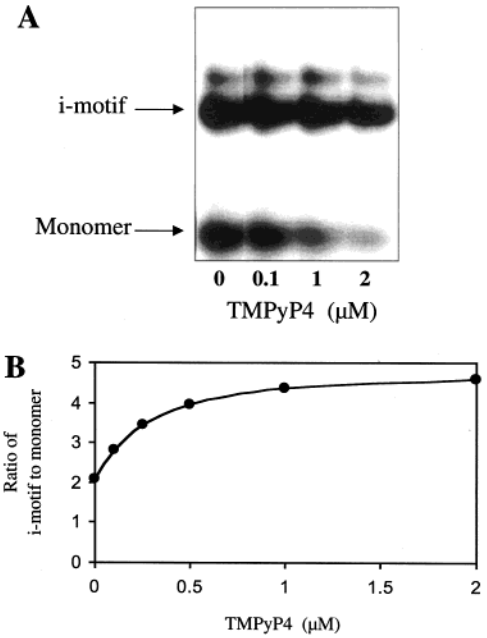

FIGURE 3: (A) Electrophoretic mobility shift assay of $(dAACCCC)_4$ with increasing concentrations of TMPyP4 (0, 0.1, 1, and 2 μM). (B) Quantification of the gel shown in panel A. The ratio of the intensities of bands corresponding to the i-motif structure vs monomer DNA in panel A is plotted vs TMPyP4 concentration.

Effect of TMPyP4 on i-Motif Formation of $(dAACCCC)_4$. The original report of the i-motif structure used polyacrylamide gel electrophoresis experiments to detect the association of oligonucleotides into a multistrand complex (*19*). This procedure can be easily adopted to study the effect of different ligands on this process. The PAGE results in Figure 3A (plotted in Figure 3B) show that overnight incubation of dAACCCC oligonucleotides with increasing concentrations of TMPyP4 enhances the yield of the aggregated form of dAACCCC. In similar experiments with potential G-quadruplex-forming oligonucleotides, we observed facilitation of the formation of G-quadruplex by several compounds, including TMPyP4 (ref *34* and a manuscript submitted for publication). Intriguingly, TMPyP4 does not increase substantially the melting point of the i-motif form (i.e., <20 °C; data not shown). It is therefore possible that it functions as a facilitator of tetraplex formation in a manner similar to the previously reported facilitation of G-quadruplex formations by some small molecules (*34*).

NMR Investigation of the TMPyP4−$(dAACCCC)_4$ *Complex.* Cationic porphyrins, including TMPyP4, present a formidable challenge for successful NMR studies of their interactions with DNA. The common problems encountered in previous studies with double-stranded DNA have been severe line broadening, porphyrin binding to the glass surface, and precipitation of the porphyrin−DNA aggregates (*35*, *36*). Thus, it was surprising that i-motif DNA produced spectra of reasonably good quality even up to equimolar concentrations of TMPyP4 and DNA. The one-dimensional NMR spectra recorded during the titration of $(dAACCCC)_4$ with TMPyP4 are shown in Figure 4. Titration was performed up to the ratio of two porphyrin molecules per DNA tetraplex. At higher ligand concentrations, the porphyrin−DNA aggregates start to precipitate. Several DNA proton

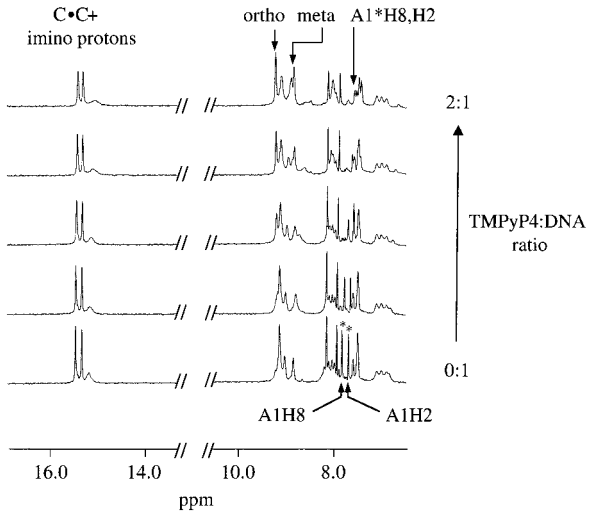

FIGURE 4: Titration of $(dAACCCC)_4$ with TMPyP4. Imino and aromatic regions of the 500 MHz NMR spectra of $(dAACCCC)_4$ are shown with increasing amounts of TMPyP4 added at 15 °C. The meta-pyridyl and ortho-pyridyl protons of TMPyP4 are labeled meta and ortho, respectively. A1H8 and A1H2 protons of free DNA are labeled below the spectra, and A1*H8 and A1*H2 protons of the complex are labeled above the spectra (an asterisk is used to distinguish the protons of the complex). Numbers at the right show the TMPyP4:DNA ratio.

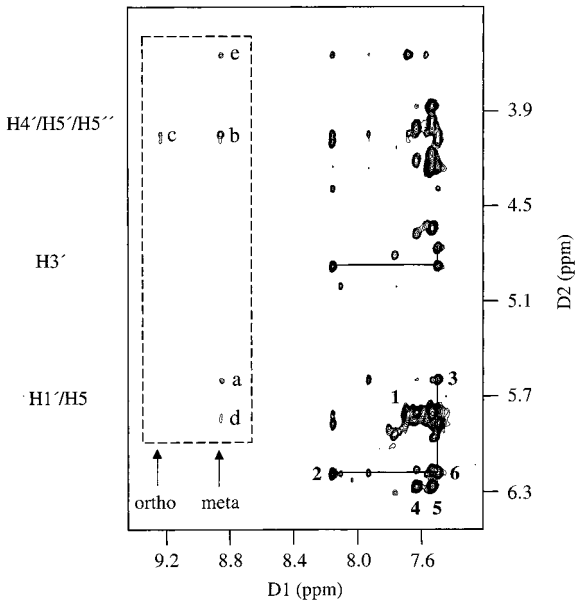

FIGURE 5: Section of the two-dimensional NOESY spectrum of the $(dAACCCC)_4$−TMPyP4 complex. The meta-pyridyl and ortho-pyridyl proton frequencies of TMPyP4 are labeled meta and ortho, respectively. Intraresidue DNA H6/H8−H1′ cross-peaks are labeled with residue numbers (1−6). Intermolecular porphyrin−DNA cross-peaks are located in the boxed region and assigned as follows: (a) C3H1′−meta-pyridyl H, (b) C3H4′−meta-pyridyl H, (c) C3H4′−ortho-pyridyl H, (d) A1H1′−meta-pyridyl H, and (e) A1H4′−meta-pyridyl H. The A2-C3 sequential connectivities in the H1′ and H3′ spectral regions are shown as solid lines.

signals in the aromatic region disappear during the titration, and a new set of resonances appears. Most dramatic are the changes in the A1H2 (0.18 ppm upfield shift) and A1H8 (0.27 ppm upfield shift) proton resonances (Figure 4). Cytosine H6 signals are also shifted upfield by 0.1−0.15 ppm (results not shown). There are no noticeable changes in the imino protons of hemiprotonated cytosines (Figure 4), suggesting that TMPyP4 neither intercalates nor stacks externally to the cytosine bases.

More direct information was obtained from two-dimensional NOESY spectra. Figure 5 shows the spectral region containing cross-peaks between aromatic and sugar protons. Several NOEs between the porphyrin and DNA protons are clearly visible. The most intense intermolecular NOEs correspond to the C3H1′−meta-pyridyl H (peak a) and the C3H4′−meta-pyridyl H (peak b) proton pairs. Weaker intermolecular NOEs were assigned to porphyrin ortho-pyridyl proton cross-peaks with C3H4′ (peak c) and meta-pyridyl proton cross-peaks with A1H1′ and A1H4′ protons (peaks d and e, respectively). The DNA structure seems to be unperturbed upon porphyrin binding since there is no significant change in the intensities of the intra-DNA cross-peaks. Most importantly, the full set of sequential connectivities between the A2 and C3 bases remains unchanged by porphyrin binding. This, as well as an absence of direct NOE connectivities between DNA base protons and the protons in the porphyrin molecule, argues against an intercalative mode of binding. The most likely binding mode, therefore, is groove binding, similar to TMPyP4 binding to AT-rich duplex DNA (*35*−*39*).

Model of the TMPyP4−(dAACCCC)₄ Complex. The groove geometry of i-motif DNA is quite different from those of other DNA forms, and this may therefore accommodate porphyrin binding better than standard double-stranded DNA structure. Specifically, the i-motif structure has two wide, shallow grooves and two very narrow grooves, with the antiparallel backbones of the intercalated C•C+ duplexes in van der Waals contact in the narrow grooves. This brings the phosphate groups of opposite strands into proximity, with intermolecular phosphorus−phosphorus distances as short as 5.9 Å (*26*). The resulting unfavorable electrostatic repulsion must be shielded by cations or bridging water molecules for the i-motif tetraplex to be stable. TMPyp4 may be ideally suited for this purpose because of its extremely high density of positive charges. Thus, the major contribution to the binding constant is likely to be electrostatic in nature. On the basis of the NMR data, we propose a model for the TMPyP4−$(dAACCCC)_4$ complex at a 2:1 ligand:tetraplex ratio, which is shown in Figure 6. This structure has been derived from restrained molecular dynamics and energy minimization simulations. Two porphyrin molecules are bound at opposite sides of the tetraplex in a symmetrical orientation. The binding geometry is close to the "face-on" binding model proposed for porphyrin binding to double-stranded DNA (*37*). One positively charged pyridyl group is anchored in the narrow groove near the C3 deoxyribose and C4 phosphate groups. The first adenine residue is partially stacked to the porphine core, which may explain the highest degree of chemical shift perturbations for this residue. The proposed model breaks the equivalence of four a priori identical AACCCC strands. However, the NMR spectra (see Figures 4 and 5) show no evidence of proton resonances splitting at a 2:1 porphyrin:tetraplex ratio, suggesting a fast equilibration between opposite porphyrin positions on the "front" and "back" sides of the tetraplex. The analogous situation has been described previously for ligand interactions with G-quadruplex DNA (*8*). There is a considerable similarity between these two systems. In each case, the ligand molecule binds to the periphery of the rigid

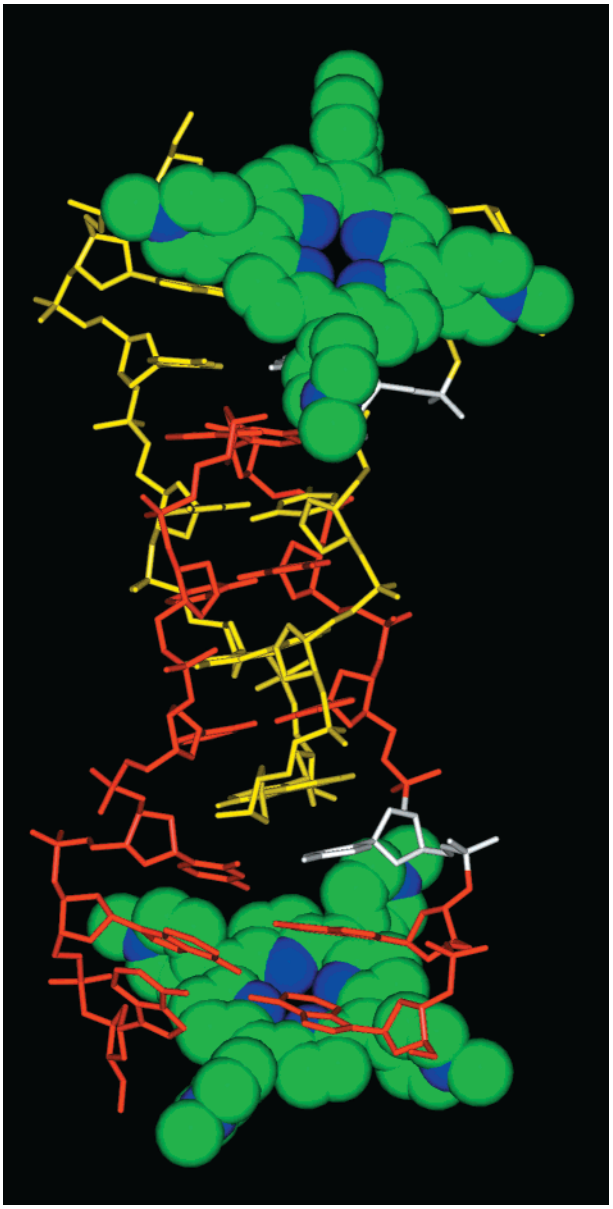

FIGURE 6: NMR-based model of the 2:1 TMPyP4−$(dAACCCC)_4$ complex. One C·C+ parallel duplex is colored yellow and the other red. C3 residues of two chains are white. TMPyP4 molecules are shown in the CPK representation. All hydrogen atoms have been omitted. The intermolecular distance restraints for C3H1′−meta-pyridyl H, C3H4′−meta-pyridyl H, C3H4′−ortho-pyridyl H, A1H1′−meta-pyridyl H, and A1H4′−meta-pyridyl H proton pairs have been applied during molecular modeling.

core of DNA tetraplex and is not impeded to exchange between symmetrical binding sites without dissociation from the DNA. An alternative explanation for the dynamic equilibrium between two identical sites is the presence of a more symmetrical static structure. We attempted to create such a model but were unable to simultaneously satisfy all the NMR restraints without the porphyrin molecule intercalating between the A2 and C3 residues, which would violate the observed strong sequential connectivity between these residues. Therefore, we favor the less symmetrical model shown in Figure 6, which is in agreement with the NOESY data.

Absorbance Spectroscopy. To obtain further insight into porphyrin binding to the i-motif, we collected UV spectra in the porphyrin Soret band upon its titration with $(dAACCCC)_4$ (Figure 7A). Pronounced bathochromic (11 nm red shift) and hypochromic (33% reduction in absorbance) effects indicate strong porphyrin binding. Titration data were analyzed using a Scatchard plot (*40*) and revealed a marked anticooperativity of binding (Figure 7B). Anticooperativity of binding and sharp isobestic points indicate the binding uniformity of several ligand molecules to the DNA tetraplex. This is consistent with the proposed model (Figure 6) where porphyrin binding to the sites symmetrical with respect to the helical axis should result in unfavorable porphyrin−porphyrin contacts. A Job-plot experiment (data not shown) indicated that there is a single high-affinity site. After this site is filled (presumably the one identified by NMR), there is a highly cooperative interaction, which given the propensity of porphyrins to self-associate could lead to the assembly of porphyrin molecules on the outside of DNA. Binding data were fitted to a neighbor exclusion model of McGhee and von Hippel (*41*). The value of the binding constant has been estimated to be 4.5×10^{-5} M, which is close to the value of TMPyP4 binding to both double-stranded (*38*, *42*) and G-quadruplex DNA (*43*−*45*).

Porphyrin Interactions with i-Motif Structures Formed by dCCCTAA and dTAACCC Telomeric Repeats. Both dCCCTAA and dTAACCC oligonucleotides form i-motif structures under standard conditions (see Materials and Methods) (Figure 8). However, the tetraplex stability is lower than that of $(dAACCCC)_4$ due to the smaller number of C·C+ pairs (*22*). In addition, both $(dCCCTAA)_4$ and $(dTAACCC)_4$ were found to exist in solution as a mixture of two forms. Two topologically different structures are most likely the "S" and "R" forms detected for the i-motif structures formed by other C-rich oligonucleotides (*33*). As mentioned above, the structural difference between these two topologies is the manner in which two C·C+ duplexes are "zipped" into each other: in the S form the 5′-end C·C+ pair is stacked on top of the 3′-end C·C+ pair of the second duplex, while in the R form the spatial arrangement of the base pairs is reversed. The relative stability of these two topologies depends on the DNA sequence, temperature, and salt conditions (*33*). The complex spectra of $(dCCCTAA)_4$ and $(dTAACCC)_4$ limit the amount of information that can be obtained from the NMR spectra of corresponding porphyrin−DNA complexes. The one-dimensional NMR spectra recorded during the titration of $(dTAACCC)_4$ and $(dCCCTAA)_4$ with TMPyP4 (panels A and B of Figure 8, respectively) show changes in DNA proton signals similar to those detected in the titration spectra of $(dAACCCC)_4$, although this time the changes in the C·C+ imino proton signals are observed, suggesting possible structural differences. The two-dimensional NOESY spectrum of the $(dTAACCC)_4$−TMPyP4 complex reveals the same pattern of intermolecular NOEs (data not shown) shown in Figure 5, which is expected since the same proposed TMPyP4 binding site on the AACC sequence segment is present in both $(dTAACCC)_4$ and $(dAACCCC)_4$ structures. However, the situation is different for the $(dCCCTAA)_4$ oligomer, where there is a 3′-overhang instead of a 5′-overhang. Consequently, the geometry of the binding should also be different. Indeed, the two-dimensional NOESY spectrum of the $(dCCCTAA)_4$−TMPyP4 complex (Figure 9) contains intermolecular NOEs both stronger and more numerous than

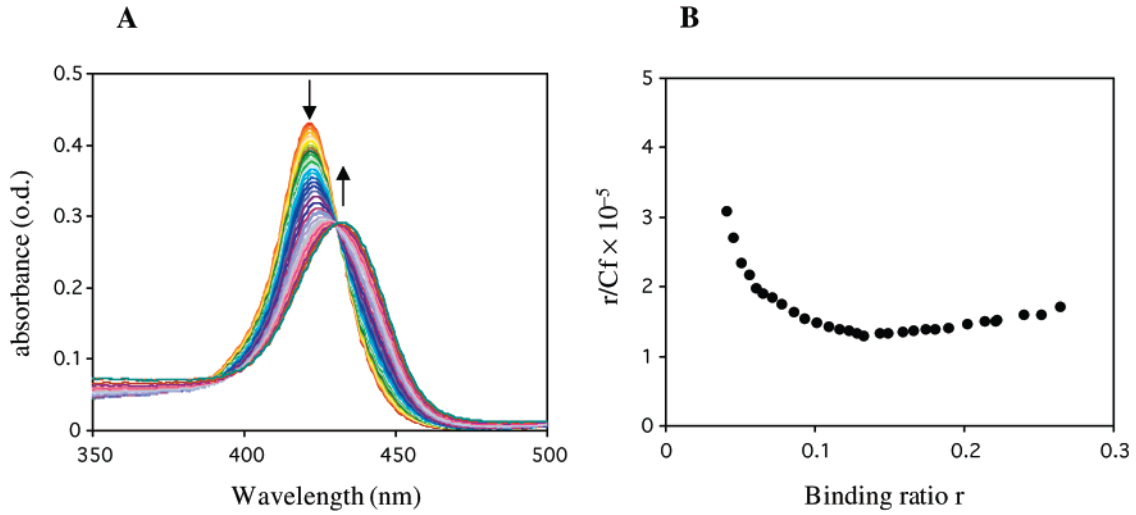

FIGURE 7: (A) UV titration of a TMPyP4 solution with $(dAACCCC)_4$. (B) Scatchard plot analysis of titration data.

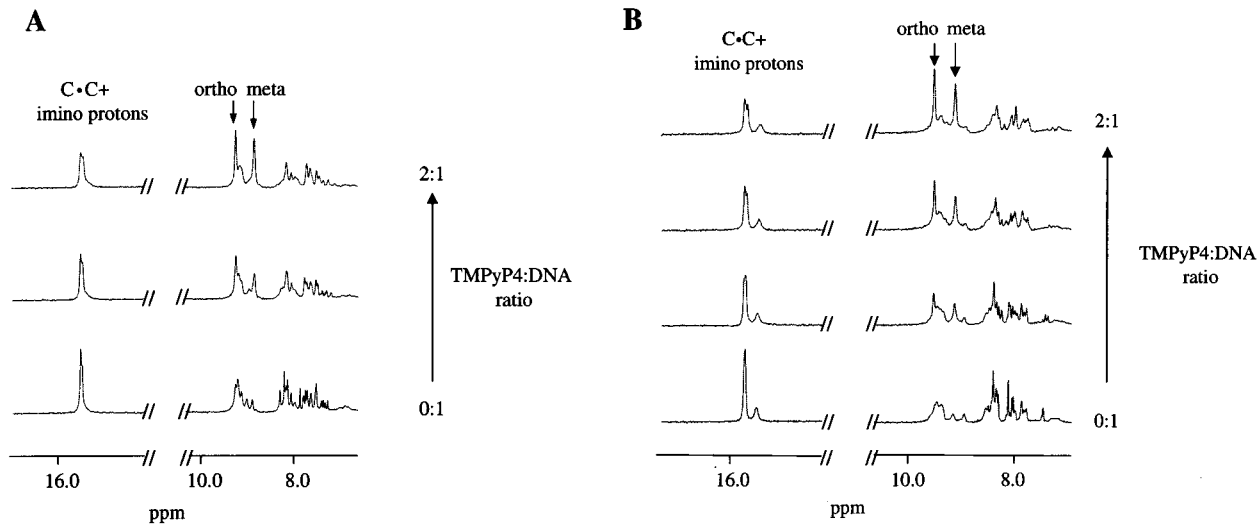

FIGURE 8: Titration of (A) $(dTAACCC)_4$ and (B) $(dCCCTAA)_4$ with TMPyP4. Imino and aromatic regions of the 500 MHz NMR are shown with increasing amounts of TMPyP4 added at 15 °C. The meta-pyridyl and ortho-pyridyl protons of TMPyP4 are labeled meta and ortho, respectively.

those found in the spectrum of either the $(dAACCCC)_4$−TMPyP4 complex or the $(dTAACCC)_4$−TMPyP4 complex. Most significant is the presence of an NOE cross-peak between the pyridyl protons and the methyl group of the thymine (peak a in Figure 9) and H2′/H2″ protons (peak b in Figure 9).

DISCUSSION

Porphyrin−DNA interactions have been extensively studied using a wide variety of techniques (*46*). Despite this, there is a limited amount of structural information about porphyrin−DNA complexes available (*36*, *47*). In the study presented here, we provide NMR measurements which provide insight into the spatial orientation of cationic porphyrins in the complex with i-motif DNA in solution.

The biological role of i-motif formation by C-rich DNA is currently uncertain. The major argument against i-motif occurrence in vivo is its marginal stability at neutral pH (*22*, *23*). It is nevertheless possible that the p*K* for i-motif formation in telomeres and other chromosomal elements can be shifted by DNA binding proteins. Therefore, there is considerable interest in the design of low-molecular weight ligands that promote i-motif formation. Through synthetic modification, there is considerable opportunity to fine-tune the structures of porphyrins and metalloporphyrins so they will interact selectively with various DNA structures, i.e., duplex DNA versus secondary structures such as G-quadruplexes (*48*) and i-motif tetraplexes. Furthermore, this may provide a unique opportunity to design ligands capable of inducing a structural transition from duplex to tetraplex DNA in functionally important regions of chromosomes (*49*). It is important to recognize that the biologically relevant i-motif DNA structures are most likely the intramolecular fold-over types rather than intermolecular complexes. Porphyrin interactions with fold-over molecules may be different than those reported here due to the influence of the structure of connecting loops. However, porphyrins interact similarly with i-motif DNA with either 5′-end extensions or 3′-end extensions (Figures 4, 5, 7, and 8). This, and the fact that the structure of the intercalated i-motif core is virtually identical in all i-motif DNA reported so far, regardless of their stoichiometry, argues in favor of a general mechanism of porphyrin binding to most if not all i-motif structures.

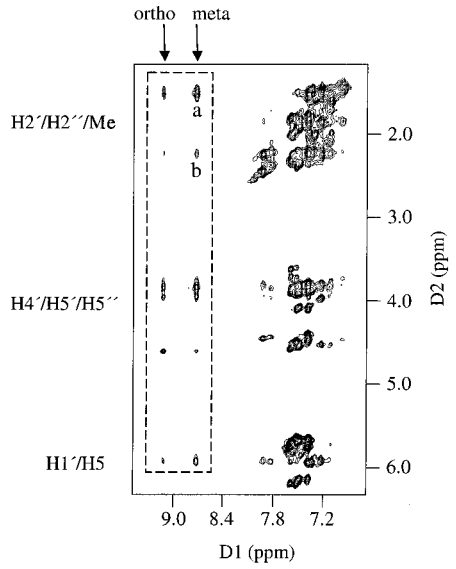

FIGURE 9: Section of the two-dimensional NOESY spectrum of the $(dCCCTAA)_4$−TMPyP4 complex. The meta-pyridyl and ortho-pyridyl protons frequencies of TMPyP4 are labeled meta and ortho, respectively. Intermolecular porphyrin−DNA cross-peaks are located in the boxed region. The cross-peak between meta-pyridyl H and the tentatively assigned T4 methyl group is labeled a, and the cross-peak between meta-pyridyl H and the tentatively assigned C3H2″ is labeled b.

Several studies have focused on the conformational transition in telomeric repeats incorporated into the plasmids (*17*, *18*, *50*). The main conclusion was the importance of pH-induced structural self-organization of the C-rich strand for any structural changes to be detected. The well-documented tendency of the G-rich strand to self-organize into G-quadruplex structures appears to be insufficient to overcome the stability of the Watson−Crick double helix under conditions of physiological superhelical density and neutral pH. Moreover, it is the stability of the C·C+-mediated structures rather than the pH-induced destabilization of Watson−Crick pairs that has been proven to be the major driving force for the conformational transition (*18*). The G- and C-rich telomeric strands can act in concert to generate stable self-paired structures, which can then be further stabilized by proteins or low-molecular weight ligands administered to cells. The crystal structure of the TMPyP4 complex with double-stranded DNA (*47*), as well as solution NMR studies (*35*, *36*), reveals that porphyrin hemi-intercalation disrupts Watson−Crick hydrogen bonds and leads to the extrusion of DNA bases from a double helix. Since TMPyP4 binds preferentially to melted or partially melted regions of DNA (*46*), it is therefore possible that porphyrins can produce structural transitions in telomeric DNA and other chromosomal regions not only by binding to G-quadruplex and i-motif structures but also by nucleation of the transition. The further tuning of cationic porphyrin structures to enhance their selectivity for G-quadruplex and i-motif tetraplexes is an important research avenue with potential clinical applications for cancer treatment (*51*, *52*, *54*).

ACKNOWLEDGMENT

Thanks to Dr. Brad Chaires for his input on the Scatchard plot. We are grateful to Dr. David M. Bishop for carefully preparing, proofreading, and editing the final version of the text and figures.

REFERENCES

1. Rhodes, D., and Giraldo, R. (1995) *Curr. Opin. Struct. Biol. 5*, 311−322.
2. Makarov, V. L., Hirose, Y., and Langmore, J. P. (1997) *Cell 88*, 657−666.
3. Wright, W. E., Tesmer, V. M., Huffman, K. E., Levene, S. D., and Shay, J. W. (1997) *Genes Dev. 11*, 2801−2809.
4. Williamson, J. R. (1994) *Annu. Rev. Biophys. Biomol. Struct. 23*, 703−730.
5. Gilbert, D. E., and Feigon, J. (1999) *Curr. Opin. Struct. Biol. 9*, 305−314.
6. Sun, D., Thompson, B., Cathers, B. E., Salazar, M., Kerwin, S. M., Trent, J. O., Jenkins, T. C., Neidle, S., and Hurley, L. H. (1997) *J. Med. Chem. 40*, 2113−2116.
7. Wheelhouse, R. T., Sun, D., Han, H., Han, F. X., and Hurley, L. H. (1998) *J. Am. Chem. Soc. 120*, 3261−3262.
8. Fedoroff, O. Yu., Salazar, M., Han, H., Chemeris, V. V., Kerwin, S. M., and Hurley, L. H. (1998) *Biochemistry 37*, 12367−12374.
9. Chung, I. K., Mehta, V. B., Spitzner, J. R., and Muller, M. T. (1992) *Nucleic Acids Res. 20*, 1973−1977.
10. Walsh, K., and Gualberto, A. (1992) *J. Biol. Chem. 267*, 13714−13718.
11. Weisman-Shomer, P., and Fry, M. (1993) *J. Biol. Chem. 268*, 3306−3312.
12. Liu, Z., and Gilbert, W. (1994) *Cell 77*, 1083−1092.
13. Frantz, J. D., and Gilbert, W. (1995) *J. Biol. Chem. 270*, 20692−20697.
14. Giraldo, R., and Rhodes, D. (1994) *EMBO J. 13*, 2411−2420.
15. Harrington, C., Lan, Y., and Akman, S. A. (1997) *J. Biol. Chem. 272*, 24631−24636.
16. Kee, K., Niu, L., and Henderson, E. (1998) *Biochemistry 37*, 4224−4234.
17. Lyamichev, V. I., Mirkin, S. M., Danilevskaya, O. N., Voloshin, O. N., Balatskaya, S. V., Dobrynin, V. N., Filippov, S. A., and Frank-Kamenetskii, M. D. (1989) *Nature 339*, 634−637.
18. Huertas, D., Lipps, H., and Azorin, F. (1994) *J. Biomol. Struct. Dyn. 12*, 79−90.
19. Gehring, K., Leroy, J. L., and Gueron, M. (1993) *Nature 363*, 561−565.
20. Leroy, J. L., Gehring, K., Kettani, A., and Gueron, M. (1993) *Biochemistry 32*, 6019−6031.
21. Leroy, J. L., Gueron, M., Mergny, J. L., and Hélène, C. (1994) *Nucleic Acids Res. 22*, 1600−1606.
22. Ahmed, S., Kintanar, A., and Henderson, E. (1994) *Nat. Struct. Biol. 1*, 83−88.
23. Manzini, G., Yathindra, N., and Xodo, L. E. (1994) *Nucleic Acids Res. 22*, 4634−4640.
24. Leroy, J. L., and Gueron, M. (1995) *Structure 3*, 101−120.
25. Kang, C., Berger, I., Lockshin, C., Ratliff, R., Moyzis, R., and Rich, A. (1995) *Proc. Natl. Acad. Sci. U.S.A. 92*, 3874−3878.
26. Berger, I., Egli, M., and Rich, A. (1996) *Proc. Natl. Acad. Sci. U.S.A. 93*, 12116−12121.
27. Nonin, S., and Leroy, J. L. (1996) *J. Mol. Biol. 261*, 399−414.
28. Nonin, S., Phan, A. T., and Leroy, J. L. (1997) *Structure 5*, 1231−1246.
29. Gallego, J., Chou, S. H., and Reid, B. R. (1997) *J. Mol. Biol. 273*, 840−856.
30. Cai, L., Chen, L., Raghavan, S., Ratliff, R., Moyzis, R., and Rich, A. (1998) *Nucleic Acids Res. 26*, 4696−4705.
31. Han, X., Leroy, J. L., and Gueron, M. (1998) *J. Mol. Biol. 278*, 949−965.
32. Izbicka, E., Nishioka, D., Marcell, V., Raymond, E., Davidson, K. K., Lawrence, R. A., Wheelhouse, R. T., Hurley, L. H., Wu, R. S., and Von Hoff, D. D. (1999) *Anti-Cancer Drug Des. 14*, 355−366.

33. Kanaori, K., Maeda, A., Kanehara, H., Tajima, K., and Makino, K. (1998) *Biochemistry 37*, 12979−12986.
34. Han, H., Cliff, C. L., and Hurley, L. H. (1999) *Biochemistry 38*, 6981−6986.
35. Marzilli, L. G., Banville, D. L., Zon, G., and Wilson, W. D. (1986) *J. Am. Chem. Soc. 108*, 4188−4192.
36. Guliaev, A. B., and Leontis, N. B. (1999) *Biochemistry 38*, 15425−15437.
37. Carvlin, M. J., Datta-Gupta, N., and Fiel, R. J. (1982) *Biochem. Biophys. Res. Commun. 108*, 66−73.
38. Carvlin, M. J., and Fiel, R. J. (1983) *Nucleic Acids Res. 11*, 6121−6139.
39. Banville, D. L., Marzilli, L. G., Strickland, J. A., and Wilson, W. D. (1986) *Biopolymers 25*, 1837−1858.
40. Scatchard, G. (1949) *Ann. N.Y. Acad. Sci. 51*, 660−674.
41. McGhee, J. D., and von Hippel, P. H. (1974) *J. Mol. Biol. 86*, 469−489.
42. Pasternack, R. F., Gibbs, E. J., and Villafranca, J. J. (1983) *Biochemistry 22*, 2406−2414.
43. Anantha, N. V., Azam, M., and Sheardy, R. D. (1998) *Biochemistry 37*, 2709−2714.
44. Haq, H., Trent, J. O., Chowdhry, B. Z., and Jenkins, T. C. (1999) *J. Am. Chem. Soc. 121*, 1768−1779.
45. Ren, J., and Chaires, J. B. (1999) *Biochemistry 38*, 16067−16075.
46. Fiel, R. J. (1989) *J. Biomol. Struct. Dyn. 6*, 1259−1274.
47. Lipscomb, L. A., Zhou, F. X., Presnell, S. R., Woo, R. J., Peek, M. E., Plaskon, R. R., and Williams, L. D. (1996) *Biochemistry 35*, 2818−2823.
48. Han, F. X., Wheelhouse, R. T., and Hurley, L. H. (1999) *J. Am. Chem. Soc. 121*, 3561−3570.
49. Rangan, A., Fedoroff, O. Yu., and Hurley, L. H. (2000) *J. Biol. Chem.* (in press).
50. Voloshin, O. N., Veselkov, A. G., Belotserkovskii, B. P., Danilevskaya, O. N., Pavlova, M. N., Dobrynin, V. N., and Frank-Kamenetskii, M. D. (1992) *J. Biomol. Struct. Dyn. 9*, 643−652.
51. Mergny, J. L., and Hélène, C. (1998) *Nat. Med. 4*, 1366−1367.
52. Mergny, J. L., Jailliet, P., Lavelle, F., Riou, J. F., Laoui, A., and Hélène, C. (1999) *Anti-Cancer Drug Des. 14*, 327−339.
53. Robidoux, S., Klinck, R., Gehring, K., and Damha, M. J. (1997) *J. Biomol. Struct. Dyn. 15*, 517−527.
54. Han, H., and Hurley, L. H. (2000) *Trends Pharmacol. Sci. 21*, 136−142.

BI001528J